Observation of a 1.979-eV spectral line of a germanium-related color center in microdiamonds and nanodiamonds

V. S. Krivobok,[1] E. A. Ekimov,[2] S. G. Lyapin,[2] S. N. Nikolaev,[1] Yu. A. Skakov,[1] A. A. Razgulov,[2,3] and M. V. Kondrin[2,*]

[1]*Lebedev Physical Institute, RAS, 117942, Leninsky Prospekt 54, Moscow, Russia*
[2]*Institute for High Pressure Physics, RAS, 108840 Troitsk, Moscow, Russia*
[3]*Moscow Institute of Physics and Technology, Dolgoprudny, Moscow Region, 141701, Russia*

(Received 18 November 2019; revised manuscript received 17 March 2020; accepted 24 March 2020; published 20 April 2020)

Color centers in diamond are considered as a platform for quantum computing and communications, biomedical markers, and nanosensors. Negatively charged split-vacancy centers have outstanding properties due to bright and almost monochromatic luminescence, but they have poor spin coherence and relaxation times. This drawback is believed to be absent in the neutral charge state of the defects. So far only the neutral silicon-vacancy center has been observed in luminescence and absorption spectra. Here we report the observation of its germanium-based analog in luminescence spectra with the zero-phonon line (ZPL) at 1.979 eV in samples containing negatively charged GeV^- centers. The relationship between the center and Ge dopant is unambiguously confirmed by studies of ^{12}C diamonds containing ^{70}Ge, ^{73}Ge, or ^{76}Ge isotopes. The intensity ratio of the ZPL of these centers varies with the crystal size, and the intensity of the GeV^0 centers reaches its maximum in samples 150 nm in size. In the vibronic sideband of this center the local vibrational mode with an energy of 23 meV was identified. The density functional theory calculations yield a ZPL energy value of the GeV^0 center which is 150 meV higher than the experimentally observed one and matches the values of its relaxational energy as well as the local phonon mode frequency.

DOI: 10.1103/PhysRevB.101.144103

I. INTRODUCTION

Impurity-vacancy complexes in diamond for a long time have attracted the attention of researchers as possible candidates for quantum computing and communications, biomedical markers, and temperature as well as magnetic-field nanosensors. Among these centers, the split-vacancy complexes are distinguished by the high Debye-Waller factor and possess bright and almost monochromatic luminescence [1]. The research on these defects is mostly focused on negatively charged complexes such as the most studied SiV^- center [2–8] and its analogs GeV^- [9–12], SnV^- [13–16], and PbV^- [17,18]. Although neutral split-vacancy centers with spin $S = 1$ are usually detected by electron paramagnetic resonance (EPR) in samples which contain SiV^- and GeV^- defects [19–23], so far, only the neutral SiV^0 center with a zero-phonon line (ZPL) at 1.31 eV has been identified in luminescence and absorption spectra [24,25]. The SiV^0 center, in comparison to its negatively charged counterpart, has a somewhat lower Debye-Waller factor (0.22 [25] vs 0.78 [26]), but on the other hand, its spin coherence and relaxation times (the features important for quantum communications) are significantly longer and can reach seconds at liquid-helium temperatures [27,28]. It is believed [1,29] that all neutrally charged split-vacancy centers possess valuable characteristics that make them interesting for quantum applications. These include the presence of an inversion center (in contrast to the NV^- center) which makes them immune to external noise and renders their spectral lines stable. The absence of partially filled degenerate energy levels in the ground state (which leads to the absence of the dynamical Jahn-Teller effect observed in the negatively charged split-vacancy centers) allows detection of EPR at room temperature and, subsequently, coherent manipulation of spins. Here we report the identification of a Ge-related optical center which has many similarities to the SiV^0 defect, and it is associated by us with the neutral charge state of the GeV center.

The structure of the split-vacancy defect consists of two vacant sites and an impurity atom located between them in the inversion center. The point group of the defect structure is D_{3d}. Six dangling bonds of carbon atoms and impurity atoms contribute ten electrons to form the electronic structure of the SiV^0 center. The transition responsible for optically active absorption at 1.31 eV consists of the promotion of one electron from the filled e_u one-electron spin-minority level to the half-filled e_g orbital and subsequent relaxation of the excited state. Two electrons on the e_u level produce the possible multielectron configuration for the ground state of $^2E_u \times {}^2E_u = {}^3A_{2g} + {}^1A_{1g} + {}^1E_g$, while for the excited states the following configuration is possible: $^2E_u \times {}^2E_g = {}^3A_{1u} + {}^3A_{2u} + {}^3E_u + {}^1A_{1u} + {}^1A_{2u} + {}^1E_u$. According to EPR measurements, the actual ground state was identified as spin-triplet $^3A_{2g}$ [19], and recent stress measurements [30] revealed that the excited

*mkondrin@hppi.troitsk.ru

state could be assigned to the ${}^3E_u$ configuration. Due to the small ZPL splitting (≈134 GHz [27]) the optical transition looks like the singlet one (and was previously ascribed to ${}^3A_{2g} \rightarrow {}^3A_{1u}$). Stress measurements also revealed dark state ${}^3A_{2u}$ 6.8 meV below the excited state. Experimental findings were recently confirmed by density functional theory calculations [29]. Due to the partially filled degenerate electron level in the excited state the split-vacancy centers (both neutral and negatively charged) are Jahn-Teller unstable [29,31], which leads to significant relaxation in the excited state and strongly influences photoluminescence spectra.

In semiconductors the charge state of the impurity depends on the position of the Fermi level, which in doped semiconductors is pinned to the charge transition level of the most abundant donors or acceptors. However, in wide-band-gap insulators such as diamond this is not usually the case, and as pointed out by Collins [32], the charge state of the defect center in diamond may be influenced by the proximity to the nearest donor (such as commonly found in synthetic diamond substitutional nitrogen). This explains why different charge states of the same color center (like NV or SiV) can be simultaneously found in the same sample. A similar charge state bimodality potentially might be observed in the split-vacancy GeV defect too.

II. METHODS

For preparation of microdiamonds with different isotopic compositions high-pressure, high-temperature (HPHT) synthesis was used ($P_{syn} = 8$–10 GPa, $T_{syn} = 1500$–1900 K). Diamonds enriched with the carbon isotope ${}^{12}C$ were synthesized from mixtures of naphthalene and Ge (C-H-Ge growth system)[12,33], while diamonds enriched with the isotope ${}^{13}C$ were produced from mixtures of Ge with amorphous carbon in the presence of distilled water (C-H-O-Ge growth system). The difference in starting materials used and chemical compositions of these two growth systems results in the same set of lines in optical spectra, which indicates their independence of the growth conditions.

Synthesis of nanodiamonds with GeV defects was carried out at a pressure of 9.4 GPa in the temperature range 1500–1700 K from mixtures of adamantane $C_{10}H_{16}$ with tetraphenylgermane $C_{24}H_{20}Ge$. The concentration of Ge was 0.004% and 0.4% with respect to a mixture of C + Ge. Parameters for the synthesis of nanodiamonds from adamantane were determined elsewhere [34]. Microcrystals 1 to 15 μm in size with 0.035% Ge were synthesized at 8 GPa and temperatures of 1900–2000 K. Characteristic morphologies of samples with nano- and microdiamonds are shown in Fig. 1, and their diffraction patterns are presented in Fig. 2. Average crystallite sizes of nanodiamonds were estimated by using the Scherrer formula for the (111) reflection in x-ray diffraction (XRD) patterns. Direct measurements of nanocrystal sizes in scanning electron microscopy pictures (Fig. 1) give values that agree well with estimates from XRD patterns. The average crystal size was 50 nm for diamonds with 0.004 at % Ge and 150 nm for crystals with 0.4 at % Ge in the growth medium. Concentrations of Ge in the growth medium correspond to the solubility limit of germanium in diamond roughly estimated earlier to be equal to 0.035% [35] for the synthesis of the 1–15-μm and 150-nm nanodiamonds, while for the synthesis of the "50-nm" sample, the dopant concentration was one order lower. We investigated samples (a) as synthesized,

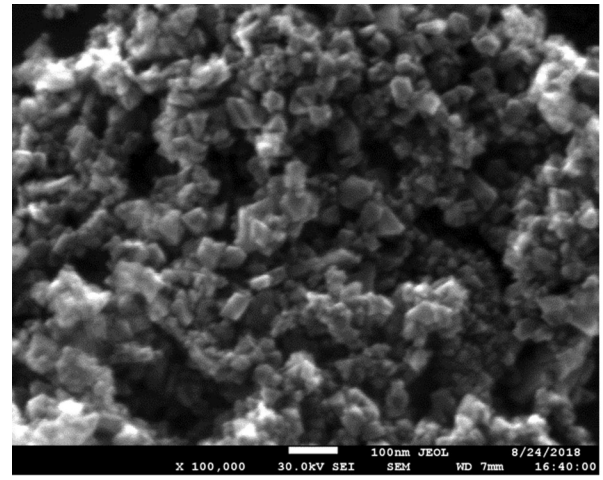

(a)

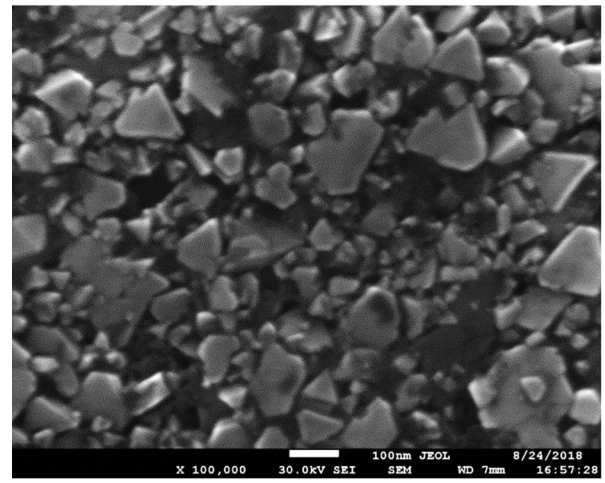

(b)

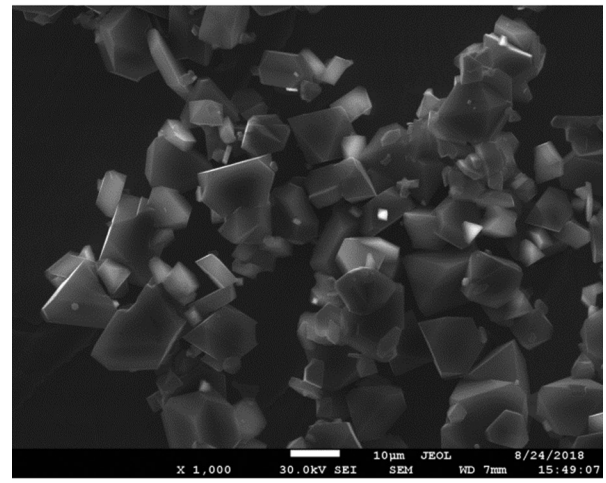

(c)

FIG. 1. Morphology of samples with (a) the 50-nm and (b) 150-nm nanodiamonds and (c) microcrystalline diamonds.

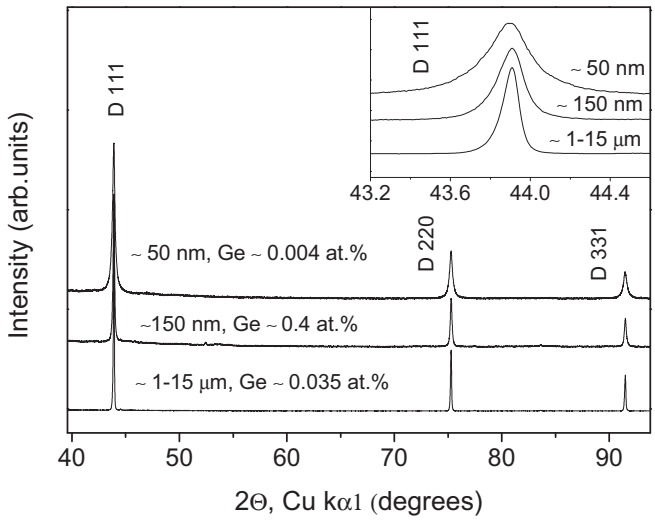

FIG. 2. XRD patterns of nano- and microcrystalline diamond samples. Broadening of the diffraction lines of nanodiamonds is clearly detected (inset).

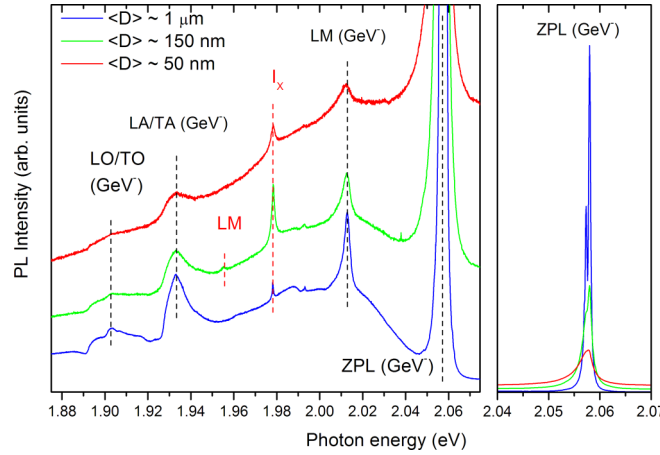

FIG. 3. Spectra of low-temperature (5 K) photoluminescence of micro- and nanocrystals of diamond in the region of radiation of the ZPL (right) of the GeV^- center and its phonon replicas (left). The average size of the crystals is shown. In all spectra, an additional line I_X is registered, the small width of which is not typical for the vibronic GeV^- peaks.

(b) after boiling in $HClO_4$ for more than 5 h, and (c) annealed in air at 720 K for 20 min, and no changes in photoluminescence spectra were detected. Since nanodiamonds start to lose intensively their mass at temperatures above 700 K in air [36], we did not use higher annealing temperatures to avoid losing nanodiamond samples.

Low-temperature emission spectra were recorded with a grating spectrograph (Princeton Instruments SpectraPro 2500, 1200 grooves/mm grating) equipped with a Pylon CCD detector (eXcelon, front illuminated). Spectral resolution better than 0.1 meV was provided by an entrance slit width of 20 μm and the same CCD pixel size. Samples were immersed in the optical cryostat (Utreks1 RTA) and cooled by continuous flow of helium vapor. A solid-state semiconductor laser (40 mW) operating at a wavelength of 472 nm was used as an excitation source. An image of the 500-μm excitation spot enlarged approximately 2.5 times was focused at the entrance slit of the spectrograph using a quartz lens (100-mm focal length). To obtain low-temperature (5 K) photoluminescence excitation spectra a grating monochromator (linear dispersion of 3.2 nm/mm) equipped with a tungsten lamp was used. In most of the experiments, the spectral resolution of this excitation source was about 0.5 nm.

The pressure effect on photoluminescence was investigated using the 488-nm Ar+ laser line for excitation and a triple-grating spectrometer (Princeton Instruments TriVista 555) with a liquid-nitrogen-cooled CCD detector. Diamond samples with a size of 10–15 μm containing GeV centers were placed in a home-built diamond-anvil cell (DAC) [37] along with a ruby crystal, serving as a pressure sensor. To ensure high hydrostaticity helium was used as a pressure-transmitting medium. For low-temperature measurements, the DAC was put into a continuous-flow cryostat (Oxford Instruments OptistatSXM), and an achromatic lens with a 100-mm focal length was used to focus the laser beam and collect the signal. The laser spot on the sample was about 5 μm.

III. RESULTS

In Fig. 3 the spectra of low-temperature (5 K) photoluminescence of small diamonds with average sizes of 50 nm, 150 nm, and ≈1 μm doped with germanium are presented. The selected spectral range includes the zero-phonon line of the GeV^- centers and the main selected peaks. As can be seen, along with the vibronic peaks corresponding to the diamond lattice (LA/TA, LO/TO) and the local phonon mode (LM) characteristic of the GeV^- center, a relatively narrow peak (I_x) is registered in the region of 1.979 eV, which was previously also attributed to the vibronic sideband of GeV^- [38]. However, this interpretation is not supported by experiments on measurement of photoluminescence spectra under conditions of resonant excitation of the GeV^- line. As seen in Fig. 4, under resonant excitation conditions, line I_X is not registered, while the structure of all other vibronic peaks is completely reproduced. To realize resonant excitation of GeV^- luminescence, we used an approximately 0.5-nm-wide spectral band with the maximum corresponding to the sharpest component of GeV^- ZPLs. In this experiment, as well as when measuring luminescence excitation spectra, we used the emission of a tungsten lamp transmitted through a grating monochromator.

The fact that line I_X is not a vibrational peak of GeV is confirmed by measurements of luminescence excitation spectra (see Fig. 5). The top two curves in Fig. 5 represent the excitation spectra of the ZPL photoluminescence and the main local phonon mode of the GeV center normalized to the maximum intensity. Except for the noise caused by a noticeably smaller luminescence signal for the local phonon mode line, these spectra reproduce each other well. The bottom two curves in Fig. 5 correspond to the excitation spectra of luminescence I_X. Since line I_X is superimposed on the vibrational band of the GeV^- center, it was necessary to subtract the background luminescence signal to obtain the excitation spectra. The red curve in Fig. 5 is obtained

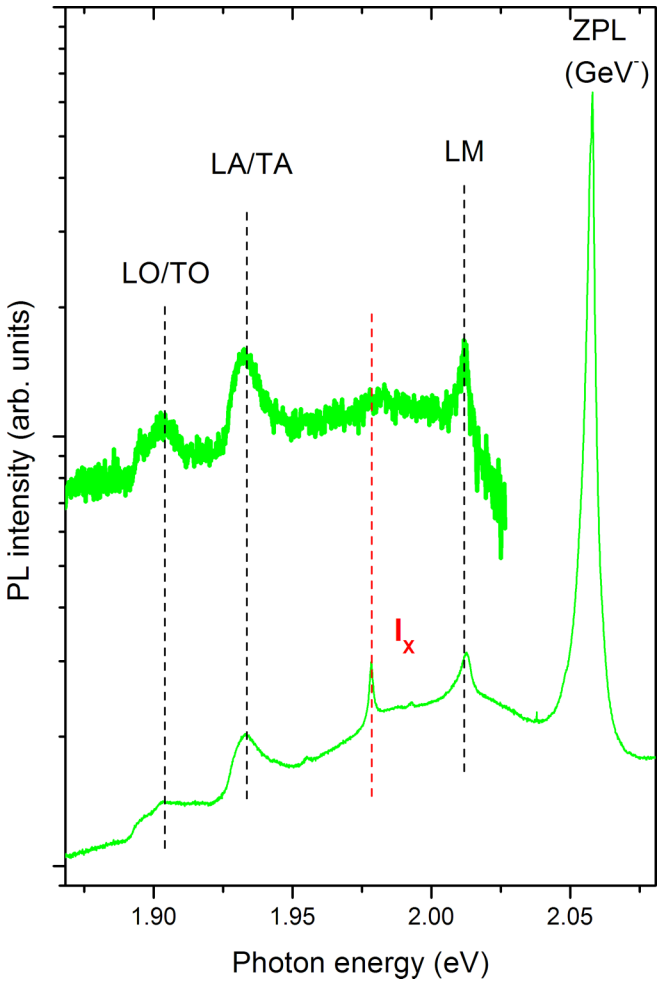

FIG. 4. Spectra of low-temperature (5 K) photoluminescence of diamond nanocrystals with an average size of 150 nm in the region of GeV-center emission under conditions of resonant excitation of the zero-phonon line (upper curve) and nonresonant excitation by radiation with a wavelength of 472 nm. Under conditions of resonant excitation, the line I_X is not registered.

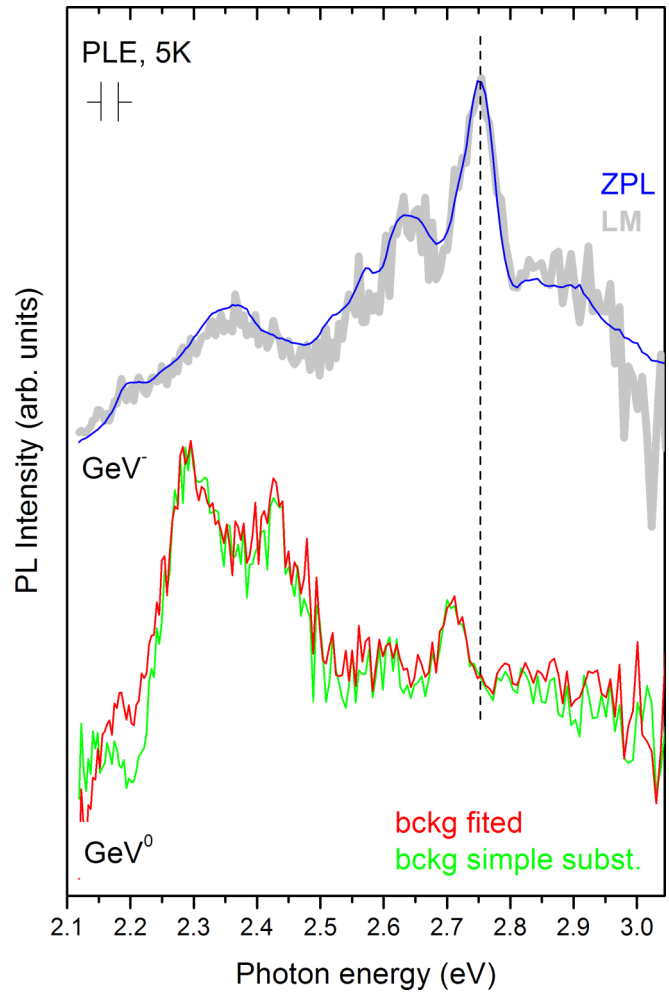

FIG. 5. Excitation spectra of luminescence at wavelengths corresponding to the I_X line (green and red curves), ZPL GeV$^-$ (blue curve), and the vibronic peak corresponding to the local phonon mode of the GeV$^-$ center (gray curve) in diamond nanocrystals with an average size of 100 nm. Since I_X is superimposed on the sideband of the GeV$^-$ center, to extract the signal I_X, we used two different subtraction procedures described in the text. All spectra are normalized to maximum intensity.

by approximating the background on both sides of line I_X, while to obtain the green curve, the background signal was determined only at the high-frequency boundary of line I_X. As seen in Fig. 5, the obtained excitation spectra are practically the same for the two described background signal subtraction procedures. At the same time, the excitation spectra of I_X differ qualitatively from the excitation spectra of ZPL GeV$^-$ and the peak corresponding to its local phonon mode. Thus, the data presented in Figs. 4 and 5 exclude a relationship between I_X and the vibronic sideband of the GeV$^-$ center.

At the same time, the connection of line I_X to the color center formed by the germanium dopant is confirmed by the analysis of photoluminescence spectra of microcrystals with different concentrations of GeV$^-$ centers and experiments on the study of microcrystals doped with different germanium isotopes. In particular, the blue dots in Fig. 6 qualitatively demonstrate the dependence of the ratio of the integral intensities for lines I_X and the ZPL of the GeV$^-$ center on the integral intensity of the latter. For the intensity of ZPL GeV$^-$ to qualitatively reflect the concentration of Ge centers we used the normalization to the Raman signal corresponding to the Γ optical phonon scattering of the diamond matrix.

Figure 6 shows that, as the intensity of ZPL (normalized to Raman signal) GeV$^-$ increases, the intensity of line I_X also monotonically increases. On the one hand, this indicates the connection of I_X to the concentration of GeV centers. On the other hand, unlike GeV$^-$ vibronic peaks, for a series of microcrystals, the signal ratio in Fig. 6 is not fixed within the experimental error. Moreover, with an increase in the intensity of ZPL GeV$^-$, a slight increase in the relative intensity I_X, which is also beyond the experimental error, is recorded. This may be due to the fact that the charge state of the GeV center is influenced by the proximity to the nearest donor. Finally, the most interesting trend is registered by the decrease in the size of the diamond crystals (see the green and red dots in Fig. 6). In this case, as follows from Fig. 3, for the intensities of ZPL GeV$^-$ and I_X lines, an opposite trend is observed:

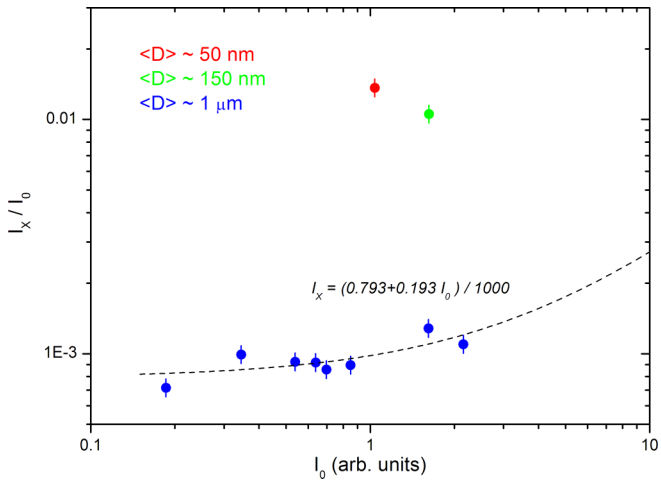

FIG. 6. The ratio of the intensity of the line I_X and ZPL GeV$^-$ depending on the integral intensity of the ZPL GeV$^-$ normalized by the value of the Raman signal corresponding to the Γ phonon scattering of the diamond matrix. The blue dots correspond to microcrystals with an average size of 1 μm. The dashed line represents the approximation of data for a microcrystal with a linear dependence. The green and red dots are data for nanocrystals with average sizes of 50 and 100 nm, the spectra of which are shown in Fig. 1.

while the intensity of ZPL GeV normalized to the Raman signal significantly decreases, the intensity of I_X increases sharply. The ratio of intensities increases by about an order of magnitude. The totality of the observations made allows preliminary identification of line I_X with another (presumably neutral) charge state of the GeV center. In this case, a sharp increase in the relative intensity of the I_X line in nanocrystals can be attributed to an effective decrease in the Fermi level in the diamond matrix due to the increasing role of surface states and electron band bending near the surface. Hydrogen surface termination, characteristic of diamonds synthesized from hydrocarbons [39], can induce a p-type surface conductive layer leading to a depletion of electrons in the impurity-vacancy defects close to the surface [40–43]. H termination of diamond withstands our efforts of surface treatment. It is known that the H-terminated surface of diamond crystals is stable in air and vacuum up to 800–900 K [44]. Hydrogen is adsorbed by the surface (111) even at a temperature of 1200 K [45]. So if H termination is present on the diamond surface, it is a very stable state.

Figure 7 illustrates the change in the spectral position of line I_X depending on the isotopic composition of the diamond matrix and the germanium dopant. Figure 7 demonstrates that as the mass of Ge increases, a gradual redshift of line I_X is observed. The dependence of the spectral position on the mass of the germanium isotope independently proves the connection of this line to the germanium centers and excludes its connection to the background impurities, the presence of which in small quantities is possible in diamond. Note that the values of isotopic shifts observed on the I_X line ($\delta E/\delta m_{Ge} = -0.053 \pm 0.01$ meV/amu and $\delta E/\delta m_C = 2.63$ meV/amu) are close to the values obtained for the GeV$^-$ center ($\delta E/\delta m_{Ge} = -0.065 \pm 0.001$ meV/amu and $\delta E/\delta m_C = 2.65$ meV/amu) [38].

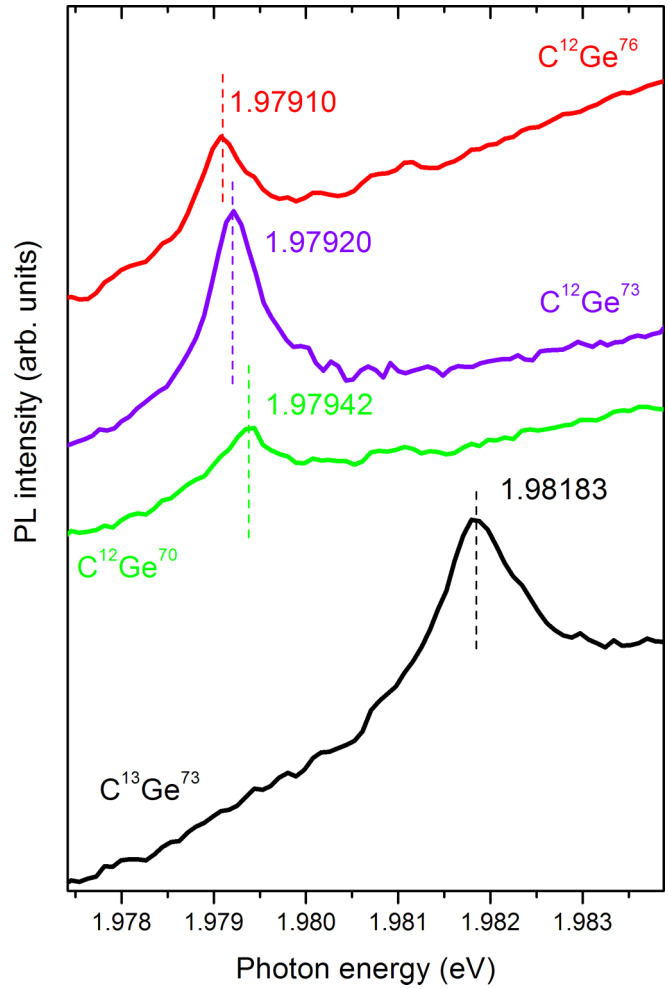

FIG. 7. The change in the spectral position of line I_X in ^{12}C diamond microcrystals doped with germanium isotopes ^{70}Ge (green curve), ^{73}Ge (purple curve), and ^{76}Ge(red curve) and in ^{13}C diamond microcrystals doped with ^{73}Ge (black curve) at a temperature of 5 K.

From Fig. 5, it follows that for the center responsible for line I_X there is an excited electronic level located in the region of ≈2.710 eV. This value falls relatively close to the energy of one of the excited levels of GeV$^-$, located in the region of 2.75 eV [46,47]. These two energy levels are convenient to use for quasiresonant excitation of the GeV$^-$ center and the center responsible for the I_X line. For Fig. 8 low-temperature photoluminescence spectra obtained under quasiresonant excitation of diamond nanocrystals ($\langle D \rangle = 150$ nm) by radiation with quantum energies of 2.709 eV and 2.753 eV are presented. The spectra in the region of the vibrational band GeV are normalized to the intensity of the peak corresponding to the local phonon mode (LM). As seen in Fig. 6, the relative intensity of line I_X increases markedly when using excitation with a quantum energy of 2.709 eV. The shape of the vibronic band of the GeV center is preserved. The result of subtracting the two normalized spectra is illustrated by the red curve in Fig. 6. Due to the fact that as a result of subtraction the contribution of vibronic peaks GeV$^-$ is negligible, the red curve allows us to estimate the vibronic band of the center related to the I_X line. As seen in Fig. 6, along with a wide band,

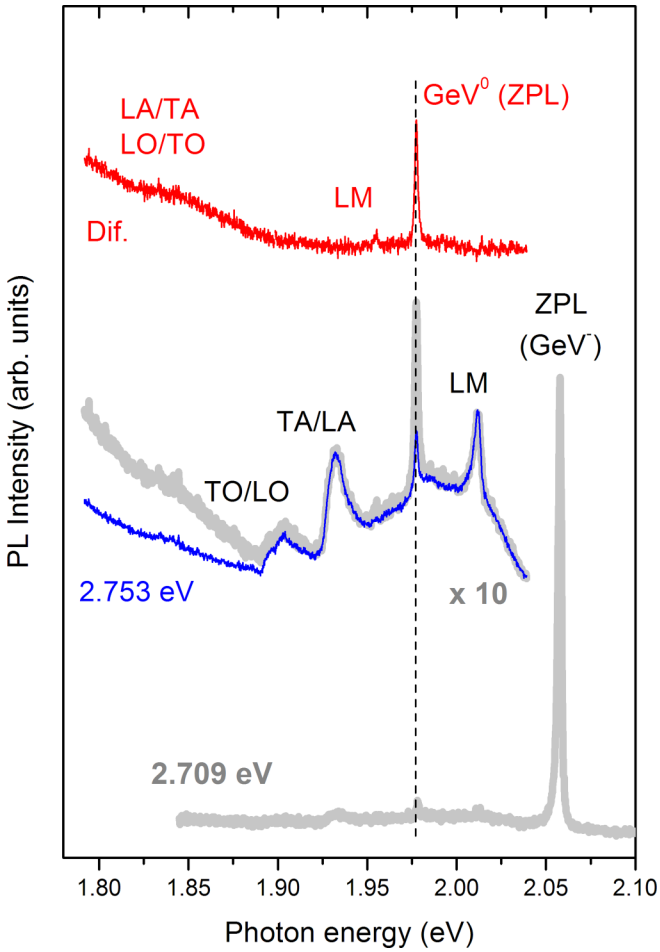

FIG. 8. Photoluminescence spectra in the emission region of the GeV^- center at a temperature of 5 K obtained when excited by radiation with a quantum energy of 2.709 eV (gray curves) and 2.753 eV (blue curve). The spectra in the region of the selected peaks are normalized to the maximum intensity of the LM line. The red curve is the result of subtracting the gray and blue curves corresponding to the spectra in the region of the GeV^- peak sideband.

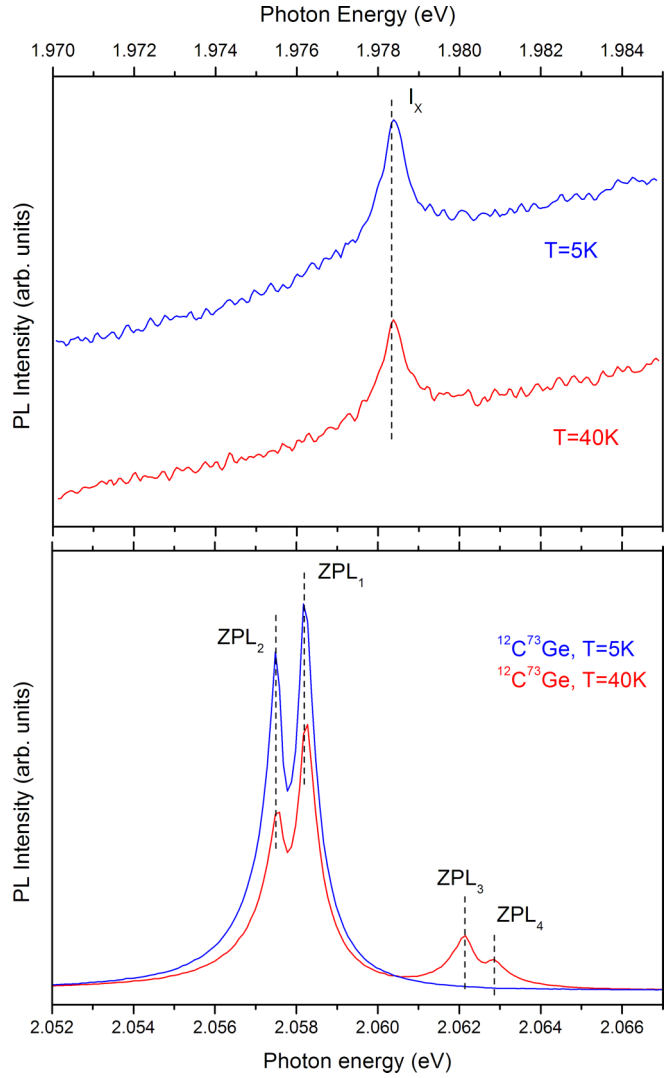

FIG. 9. Emission spectra in region I_X (top) and the ZPL GeV^- (bottom) recorded at temperatures of 5 K (blue curves) and 40 K (red curves) for $^{12}C\,^{73}Ge$ microcrystals.

which can be interpreted as phonon replicas governed by optical and acoustic phonons of the diamond matrix (LA/TA, LO/TO), a relatively narrow satellite peak shifted relative to I_X by ≈23 meV is registered in the difference spectrum. This peak, also recorded on the blue curve in Fig. 3, corresponds, apparently, to the local phonon mode.

For split-vacancy SiV^- and GeV^- complexes, the presence of a fine structure in the ground and excited states is a characteristic feature. This splitting results in the formation of four components of a fine structure, which are clearly observed at low temperatures. An example of such a fine structure is shown in Fig. 9 (bottom) for GeV centers in $^{12}C\,^{73}Ge$ microcrystals. At the same time, as can be seen from this figure, for line I_X in the same sample, no evidence of a fine structure is revealed.

Additional support that the I_X line can be attributed to the neutral GeV center comes from the pressure evolution of the I_X line. As seen in Fig. 10, a pressure increase in the range up to 6 GPa leads to a practically linear blueshift in the energy of the I_X line. The fitting of available data yields a pressure coefficient of 2.9 ± 0.03 meV/GPa, which is comparable but slightly less than the pressure coefficient of GeV^- ZPL $[\delta E(GeV^-)/\delta P = 3.11 \pm 0.03\,\text{meV/GPa}]$ [48]. The calculated pressure coefficient of the neutral GeV center is also less than the value of the GeV^- center, which is remarkably close to the experimentally observed value, but the predicted coefficient is slightly higher $[\delta E(GeV^0)/\delta P = 3.0\,\text{meV/GPa}]$ [49].

IV. DISCUSSION

In a recent work, Thiering and Gali [29] predicted the ZPL energy of the GeV^0 center to be 1.798 eV, which is almost 180 meV below the I_X line with an energy of 1.979 eV. The observed error is greater than the value of 100 meV admissible in this type of density functional theory (DFT) calculation. To investigate the possible origin of this discrepancy we made our own calculations of the neutral GeV center.

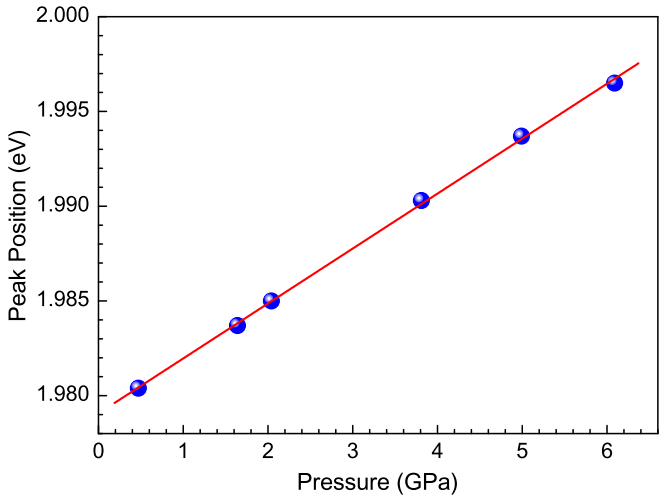

FIG. 10. Pressure dependence of the I_X line.

In *ab initio* calculations the QUANTUM ESPRESSO software package was used [50]. The impurity center was modeled in 83- and 216-atom periodic supercells having C_{3i} point group symmetry. For the density functional calculation we employed the Perdew-Burke-Ernzerhof exchange correlation method with norm-conserving pseudopotentials for both carbon and impurity atoms with an energy cutoff of 70 Ry. Before the calculation of electronic states, the crystal lattice and atom positions were fully optimized until the residual force on every atom became less than 0.001 Ry/bohr. After that additional calculations were performed in the obtained geometry using the hybrid Heyd-Scuseria-Ernzerhof (HSE06) functional to clarify the position of impurity levels in the electronic band gap. For this kind of calculation energy sampling only in the center of the Brillouin zone was done. To calculate the relaxational energy of the excited state the Delta self-consistent field (ΔSCF) method was used with an inverted population of electron levels and subsequent geometry optimization with the same parameters as for the ground state. To calculate the excited state of the GeV^- center the uniform distribution of electrons in the e_u and e_g electron orbitals in the spin-minority channel was used. Such a uniform distribution models the occupation of electron levels at high temperatures. Vibrational properties of the defect center were obtained by calculating the energy of the impurity atom shifted along the axis connecting the two vacant sites in split-vacancy centers or in the plane normal to it with the positions of all carbon atoms fixed. This corresponds to calculations of the frequencies of the A_{2u} and E_u quasilocal phonon modes, respectively. In this sort of calculation the "minimal" assumption about vibronic properties was adopted, and it was assumed that the local mode does not involve the oscillation of carbon atoms. In the GeV^- center, this assumption is also corroborated by experimental findings on isotopic substitution of carbon and impurity atoms [38].

The calculated vertical excitation energy for the GeV^0 center was 2.22 eV, which is close to the value of 2.134 eV obtained in Ref. [29]. However, the relaxation energy calculated by us (91 meV) is far below the value of 242 meV predicted earlier [29]. So the ZPL energy of the GeV^0 center according to our calculation is 2.13 eV, which is 150 meV above that experimentally observed. Due to the complex nature of the excited state of the center (which is a product Jahn-Teller system) the small relaxation energy may be related to the fact that the system during geometry optimization was trapped in the local minimum and the real relaxation energy would be greater. The value of relaxation energy does influence the value of the Huang-Rhys factor and, subsequently, the intensity of vibronic sideband. To estimate the Huang-Rhys factor one should evaluate the energy of vibrational quanta.

Oscillations of the impurity atom lead to the appearance of the sharp local phonon modes in the wings of the luminescence spectra of the defect center. Due to the trigonal symmetry of the defect two vibrational modes are expected with A_{2u} and E_u symmetries. Calculations yield their energies to be 28.63 and 38.72 meV, respectively. According to the Franck-Condon principle for a certain mode to be present in the vibrational sideband some kind of distortion should take place. Obviously, in our case the distortions consist of shifting the impurity atom along the trigonal axis (which leads to the loss of inversion symmetry and makes visible the A_{2u} mode) in the excited electronic state. The corresponding distortion is, indeed, observed in calculations. Subduction of the D_{3d} point group to C_{3v} reduces A_{2u} representation to the trivial and most symmetric one. A similar pattern is observed in the SiV^0 center, where of two possible modes (with calculated energies of 46.54 and 61.13 meV) only one local vibrational mode with a measured frequency of 39 meV is visible [30]. It should be noted that a different type of distortion is observed in the negatively charged split-vacancy center SiV^-, where the local vibrational mode has E_u symmetry [51]. Apparently, the difference between two charged states of structurally the same split-vacancy center is connected to the different types of Jahn-Teller instability occurring in them: the product Jahn-Teller effect is observed in the excited state of the neutral complex [29], and the dynamical Jahn-Teller effect is present in the ground and excited states of the negatively charged center [31].

Although the local vibrational mode is very spectacular in the luminescence sideband of the split-vacancy center, due to its small relative integral intensity it has only a minor effect on the overall Debye-Waller factor. The major contribution to the vibronic sideband comes from the distortions the defect center exerts on the diamond crystal lattice. It was noticed before that the vibronic sideband of defect centers with different structures has certain similarities to and features that can be ascribed to Van Hove singularities in the density of states of bulk phonons [38,52]. So to estimate the Huang-Rhys factor S one can use the formula $S = E_R/\hbar\omega$, where E_R is the relaxation energy of the defect center in the excited state and $\hbar\omega$ is the average phonon frequency in pure diamond. This frequency can be evaluated using the phonon density of states of pure diamond and equals approximately 95 meV. The low-temperature Debye-Waller factor is connected to the Huang-Rhys one by the relation $I_{ZPL}/(I_{SB} + I_{ZPL}) = \exp(-S)$. Application of these formulas yields the experimental assessments of relaxation energies in SiV^0 and SiV^- centers to be 142 and 25 meV, respectively. The Debye-Waller factor of the GeV^- center is approximately 0.65, which corresponds to a relaxation energy of 41 meV. This value can

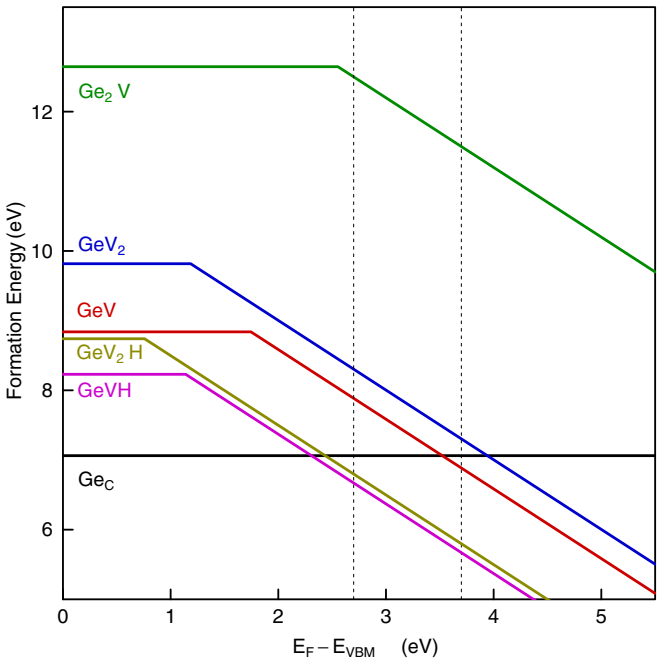

FIG. 11. Dependence of the formation energy of the substitutional germanium atom and three impurity vacancy complexes in neutral and negative charge states on the Fermi level E_F (relative to valence band maximum E_{VBM}). The kinks in the dependencies mark the $(0|-)$ charge transition level. Vertical dashed lines mark positions of the Fermi level in pure (2.7 eV) diamond and typical HPHT diamond doped with substitutional nitrogen (3.7 eV).

be compared with the direct experimental estimation of the relaxation energy calculated as the barycenter of the luminescence sideband [53]:

$$E_R = E_{ZPL} - \frac{\int I(E)dE/E^2}{\int I(E)dE/E^3},$$

where $I(E)$ is the experimental intensity of the phonon sideband. The value is equal to 29 meV, which is, by order of magnitude, comparable with the value obtained earlier and gives a rough assessment of errors introduced by approximations. Moreover, the low relaxation energy of negatively charged split-vacancy centers is corroborated by DFT calculations [31]. The estimation of the Debye-Waller factor of luminescence spectra depicted in Fig. 8 yields a value of 0.3, which corresponds to a relaxation energy of 114 meV. The calculated values of relaxation energies of neutral split-vacancy centers are greater than their negatively charged counterparts, but they are almost 100 meV below the values predicted by DFT methods in Ref. [29]. Still, for the GeV^0 center this energy is close to the value calculated by us.

However, there is a small possibility that the I_X line is related to a defect center different from the GeV one. For this purpose we calculated the formation energy of substitutional germanium, the GeV center, and two larger aggregates, GeV_2 and $\mathrm{Ge}_2\mathrm{V}$, in neutral and negatively charged states. Because we cannot exclude the influence of hydrogen on the resulting impurity-vacancy complexes, we consider their hydrogenated counterparts too (see Fig. 11). The formation energy of the defect in the charge state q is defined as

$$E_f^q(E_F) = E_{\mathrm{tot}}^q - \sum_{C,Ge,H} n_i\mu_i - q(E_F - E_{\mathrm{VBM}}) + E_{\mathrm{corr}}^q,$$

where μ_C and μ_{Ge} are the chemical potentials of carbon and germanium calculated in pure bulk materials. μ_H is half of the hydrogen molecule energy. The Fermi level E_F is calculated with respect to the valence band maximum E_{VBM} of the pure host lattice. The upper limit of the correction term E_{corr}^q was taken to be the monopole contribution to the Makov-Payne correction, which for a 216-atom lattice and singly negatively charged defect is equal to 0.35 eV. The formation energy E_f quantifies the thermodynamic probability of defect center formation, and thereafter the relative concentration of the defect $[X] \propto \exp(-E_f(X)/kT_{\mathrm{syn}})$, where T_{syn} is the synthesis temperature. This value does not take into account kinetic issues which cause the formation of large aggregates to have a long synthesis time (instead of the few minutes typical of our process) or large annealing temperatures. For example, aggregation of substitutional nitrogen into A (two adjacent nitrogen atoms) and B (four nitrogen atoms surrounding a vacancy) centers in synthetic diamonds requires annealing temperatures above 1700 K and several hours to complete [54]. So we restrict our consideration to the smallest possible aggregates consisting of three elemental defects: vacancies and impurity atoms. It is interesting to note that the formation energy of nitrogen aggregates decreases with the aggregate's size: for A and B centers it is approximately equal to the energy of substitutional nitrogen (3.59 eV) [55] and is lower than the formation energy of the neutral NV center (6.21 eV) [56]. The opposite trend is observed in Ge-related complexes (Fig. 11), where the formation energy of the neutral GeV center is lower than formation energies of neutral GeV_2 and $\mathrm{Ge}_2\mathrm{V}$ defects.

The substitutional germanium is isoelectronic with the host, so the only effect it produces on the electronic structure of diamond is to push up the valence band maximum [5]. Its formation energy is lower than that of the GeV center (so it should be found in a larger concentration than the latter one), but this defect is diamagnetic and optically and electrically inactive (it exists only in a neutral state), so it is almost invisible to physical methods of investigation. The formation energy of the $\mathrm{Ge}_2\mathrm{V}$ center [the structural analog of H2 or H3 nitrogen-containing centers with $C_{2v}(mm2)$ symmetry] is too high for it to be present in appreciable quantities. The only aggregate energetically competitive with a negatively charged GeV center in the range of realistic values of the Fermi level is paramagnetic GeV_2^-. Its silicon-related counterpart was theoretically studied before [57,58] but, as far as we know, was not identified in experiments. Structurally, it consist of a GeV defect in the split-vacancy position located near a second vacancy. The overall symmetry of the defect is $C_s(m)$. It is optically active in the infrared range. DFT calculations suggest that the luminescence caused by promotion of an electron from the highest fully occupied energy level to the lowest unoccupied one in spin-minority and spin-majority channels (see Fig. 12) results in ZPLs with energies of 1.17 and 1.46 eV and relaxation energies of 81 and 68 meV, respectively.

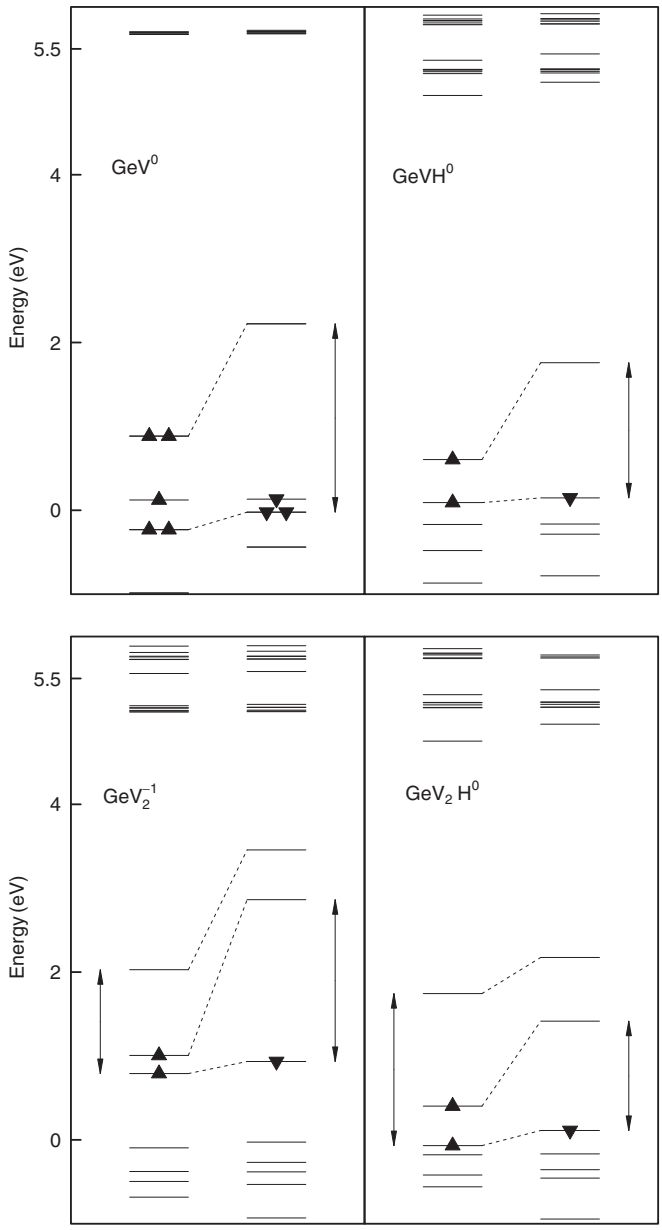

FIG. 12. The Kohn-Sham orbitals of GeV and related centers. Up and down triangles mark the highest occupied orbitals in spin-majority and spin-minority channels, respectively. Arrows designate the optically active electronic transitions considered in the text.

The hydrogenated counterparts of GeV and GeV_2 defects are analogs of registered in EPR measurements the $SiVH^0$ and SiV_2H^0 centers (KUL3 and WAR3, respectively) [19,24,59] observed on samples grown using the chemical vapor deposition method. Later on, the optical absorption line with an energy of 1.018 eV was ascribed to the negatively charged SiV_2H^- center [58], but so far the KUL3 center has not been identified in photoluminescence or absorption. Taking the lower solubility of Ge in HPHT diamond compared with that of Si, detection of germanium-hydrogen defects in Photoluminescence becomes even less realistic, leaving space for theoretical calculations to investigate these possibilities.

As follows from Fig. 11, the energies of both neutral and negatively charged GeVH and GeV_2H centers with $C_s(m)$ symmetry are lower than the energy of the GeV^0 center, so all of them should be considered as possible candidates for the I_X line. The calculated positions of Kohn-Sham levels of paramagnetic neutral hydrogen containing centers are depicted in Fig. 12. For the $GeVH^0$ center the transition marked in Fig. 12 has an energy of 1.20 eV with a relaxation contribution of 120 meV. For GeV_2H^0 the calculated ZPL energies are 1.38 eV (with 68-meV relaxation energy) and 0.74 eV (with 73 meV relaxation energy) in spin-majority and spin-minority channels, respectively. In negative charge states both centers are diamagnetic. An additional electron fills the partially occupied level and aligns spin-up and spin-down orbitals on the energy level diagram. So the only possible excitation for the $GeVH^-$ center is to free orbitals close to the conduction band minima and has an energy above 3 eV. For GeV_2H^- the excitation between the highest partially filled orbital and the lowest free one is 1.08 eV with a relaxation energy of 73 meV.

The low values of calculated ZPL energies demonstrate that GeV_2^-, GeVH, and GeV_2H defects cannot be responsible for the experimentally observed optical line with an energy of 1.979 eV.

V. CONCLUSIONS

Optical measurements reveal the existence of a luminescence peak with a ZPL energy of 1.979 eV. Isotopic substitution of dopant atoms demonstrates that the observed luminescence peak is related to the germanium-based defect. Independent excitation of the luminescence of this center and a nearby ZPL of the negatively charged GeV^- center proves that this line does not belong to the luminescence sideband of the GeV^- complex. The intensity of this peak strongly depends on the size of the crystal and reaches its maximum in the nanodiamonds with a crystal size equal to 150 nm. The peak is an optical singlet, and low-temperature measurements do not reveal any fine structure with a frequency splitting above 250 GHz. The peak is accompanied by a weak satellite attributed to the local vibrational mode with an oscillation energy of 23 meV. The experimental Debye-Waller factor of this center is roughly estimated to be around 0.3. The quasisinglet optical transition, the small energy of the local mode, and the relatively low Debye-Waller factor resemble the SiV^0 center. All experimental evidence allows us to tentatively attribute the center under consideration to the neutral charge state of the GeV complex. This conclusion is corroborated by isotopic and pressure shifts of the ZPL of the GeV^0 center. *Ab initio* calculations of the GeV^0 center yield a value of ZPL energy equal to 2.13 eV, which is in tolerable agreement with the experimental one. The calculated relaxational energy (91 meV) roughly matches one obtained from the experimental Debye-Waller factor.

ACKNOWLEDGMENT

This work is supported by the Russian Science Foundation (Grant No. 19-12-00407).

[1] D. Chen, N. Zheludev, and W.-b. Gao, Adv. Quantum Technol. **3**, 1900069 (2020).

[2] V. S. Vavilov, A. A. Gippius, A. M. Zaitsev, B. V. Deryagin, B. V. Spitsyn, and A. E. Aleksenko, Fiz. Tekh. Poluprovodn. **14**, 1811 (1980) [Sov. Phys. Semicond. **14**, 1078 (1980)].

[3] C. D. Clark, H. Kanda, I. Kiflawi, and G. Sittas, Phys. Rev. B **51**, 16681 (1995).

[4] J. P. Goss, R. Jones, S. J. Breuer, P. R. Briddon, and S. Öberg, Phys. Rev. Lett. **77**, 3041 (1996).

[5] J. P. Goss, P. R. Briddon, M. J. Rayson, S. J. Sque, and R. Jones, Phys. Rev. B **72**, 035214 (2005).

[6] C. Hepp, T. Müller, V. Waselowski, J. N. Becker, B. Pingault, H. Sternschulte, D. Steinmüller-Nethl, A. Gali, J. R. Maze, M. Atatüre, and C. Becher, Phys. Rev. Lett. **112**, 036405 (2014).

[7] L. J. Rogers, K. D. Jahnke, M. W. Doherty, A. Dietrich, L. P. McGuinness, C. Müller, T. Teraji, H. Sumiya, J. Isoya, N. B. Manson, and F. Jelezko, Phys. Rev. B **89**, 235101 (2014).

[8] L. J. Rogers, K. D. Jahnke, M. H. Metsch, A. Sipahigil, J. M. Binder, T. Teraji, H. Sumiya, J. Isoya, M. D. Lukin, P. Hemmer, and F. Jelezko, Phys. Rev. Lett. **113**, 263602 (2014).

[9] T. Iwasaki, F. Ishibashi, Y. Miyamoto, Y. Doi, S. Kobayashi, T. Miyazaki, K. Tahara, K. D. Jahnke, L. J. Rogers, B. Naydenov, F. Jelezko, S. Yamasaki, S. Nagamachi, T. Inubushi, N. Mizuochi, and M. Hatano, Sci. Rep. **5**, 12882 (2015).

[10] Y. N. Palyanov, I. N. Kupriyanov, Y. M. Borzdov, and N. V. Surovtsev, Sci. Rep. **5**, 14789 (2015).

[11] V. G. Ralchenko, V. S. Sedov, A. A. Khomich, V. S. Krivobok, S. N. Nikolaev, S. S. Savin, I. I. Vlasov, and V. I. Konov, Bull. Lebedev Phys. Inst. **42**, 165 (2015).

[12] E. A. Ekimov, S. G. Lyapin, K. N. Boldyrev, M. V. Kondrin, R. Khmelnitskiy, V. A. Gavva, T. V. Kotereva, and M. N. Popova, JETP Lett. **102**, 701 (2015).

[13] T. Iwasaki, Y. Miyamoto, T. Taniguchi, P. Siyushev, M. H. Metsch, F. Jelezko, and M. Hatano, Phys. Rev. Lett. **119**, 253601 (2017).

[14] S. D. Tchernij, T. Herzig, J. Forneris, J. Küpper, S. Pezzagna, P. Traina, E. Moreva, I. P. Degiovanni, G. Brida, N. Skukan, M. Genovese, M. Jakšić, J. Meijer, and P. Olivero, ACS Photonics **4**, 2580 (2017).

[15] E. Ekimov, S. Lyapin, and M. Kondrin, Diamond Relat. Mater. **87**, 223 (2018).

[16] Y. N. Palyanov, I. N. Kupriyanov, and Y. M. Borzdov, Carbon **143**, 769 (2019).

[17] S. Ditalia Tchernij, T. Lühmann, T. Herzig, J. Küpper, A. Damin, S. Santonocito, M. Signorile, P. Traina, E. Moreva, F. Celegato, S. Pezzagna, I. P. Degiovanni, P. Olivero, M. Jakšić, J. Meijer, P. M. Genovese, and J. Forneris, ACS Photonics **5**, 4864 (2018).

[18] M. E. Trusheim, N. H. Wan, K. C. Chen, C. J. Ciccarino, J. Flick, R. Sundararaman, G. Malladi, E. Bersin, M. Walsh, B. Lienhard, H. Bakhru, P. Narang, and D. Englund, Phys. Rev. B **99**, 075430 (2019).

[19] A. M. Edmonds, M. E. Newton, P. M. Martineau, D. J. Twitchen, and S. D. Williams, Phys. Rev. B **77**, 245205 (2008).

[20] V. Nadolinny, A. Komarovskikh, Y. Palyanov, I. Kupriyanov, Y. Borzdov, M. Rakhmanova, O. Yuryeva, and S. Veber, Phys. Status Solidi A **213**, 2623 (2016).

[21] V. A. Nadolinny, A. Y. Komarovskikh, Y. N. Palyanov, I. N. Kupriyanov, Y. M. Borzdov, M. I. Rakhmanova, O. P. Yuryeva, and S. L. Veber, J. Struct. Chem. **57**, 1041 (2016).

[22] A. Komarovskikh, A. Dmitriev, V. Nadolinny, and Y. Palyanov, Diamond Relat. Mater. **76**, 86 (2017).

[23] A. Komarovskikh, M. Uvarov, V. Nadolinny, and Y. Palyanov, Phys. Status Solidi A **215**, 1800193 (2018).

[24] U. F. S. D'Haenens-Johansson, A. M. Edmonds, M. E. Newton, J. P. Goss, P. R. Briddon, J. M. Baker, P. M. Martineau, R. U. A. Khan, D. J. Twitchen, and S. D. Williams, Phys. Rev. B **82**, 155205 (2010).

[25] U. F. S. D'Haenens-Johansson, A. M. Edmonds, B. L. Green, M. E. Newton, G. Davies, P. M. Martineau, R. U. A. Khan, and D. J. Twitchen, Phys. Rev. B **84**, 245208 (2011).

[26] E. Neu, C. Hepp, M. Hauschild, S. Gsell, M. Fischer, H. Sternschulte, D. Steinmüller-Nethl, M. Schreck, and C. Becher, New J. Phys. **15**, 043005 (2013).

[27] B. L. Green, S. Mottishaw, B. G. Breeze, A. M. Edmonds, U. F. S. D'Haenens-Johansson, M. W. Doherty, S. D. Williams, D. J. Twitchen, and M. E. Newton, Phys. Rev. Lett. **119**, 096402 (2017).

[28] B. C. Rose, D. Huang, Z.-H. Zhang, P. Stevenson, A. M. Tyryshkin, S. Sangtawesin, S. Srinivasan, L. Loudin, M. L. Markham, A. M. Edmonds, D. J. Twitchen, S. A. Lyon, and N. P. de Leon, Science **361**, 60 (2018).

[29] G. Thiering and A. Gali, npj Comput. Mater. **5**, 18 (2019).

[30] B. L. Green, M. W. Doherty, E. Nako, N. B. Manson, U. F. S. D'Haenens-Johansson, S. D. Williams, D. J. Twitchen, and M. E. Newton, Phys. Rev. B **99**, 161112(R) (2019).

[31] G. Thiering and A. Gali, Phys. Rev. X **8**, 021063 (2018).

[32] A. T. Collins, J. Phys.: Condens. Matter **14**, 3743 (2002).

[33] V. A. Davydov, A. V. Rakhmanina, S. G. Lyapin, I. D. Ilichev, K. N. Boldyrev, A. A. Shiryaev, and V. N. Agafonov, JETP Lett. **99**, 585 (2014).

[34] E. A. Ekimov, O. S. Kudryavtsev, N. E. Mordvinova, O. I. Lebedev, and I. I. Vlasov, ChemNanoMat **4**, 269 (2018).

[35] E. Ekimov, M. Kondrin, V. Krivobok, A. Khomich, I. Vlasov, R. Khmelnitskiy, T. Iwasaki, and M. Hatano, Diamond Relat. Mater. **93**, 75 (2019).

[36] S. Osswald, M. Havel, V. Mochalin, G. Yushin, and Y. Gogotsi, Diamond Relat. Mater. **17**, 1122 (2008).

[37] A. P. Novikov, S. G. Lyapin, and S. M. Stishov, Instrum. Exp. Tech. **62**, 136 (2019).

[38] E. A. Ekimov, V. S. Krivobok, S. G. Lyapin, P. S. Sherin, V. A. Gavva, and M. V. Kondrin, Phys. Rev. B **95**, 094113 (2017).

[39] O. S. Kudryavtsev, E. A. Ekimov, A. M. Romshin, D. G. Pasternak, and I. I. Vlasov, Phys. Status Solidi A **215**, 1800252 (2018).

[40] K.-M. C. Fu, C. Santori, P. E. Barclay, and R. G. Beausoleil, Appl. Phys. Lett. **96**, 121907 (2010).

[41] M. V. Hauf, B. Grotz, B. Naydenov, M. Dankerl, S. Pezzagna, J. Meijer, F. Jelezko, J. Wrachtrup, M. Stutzmann, F. Reinhard, and J. A. Garrido, Phys. Rev. B **83**, 081304(R) (2011).

[42] K. Groot-Berning, N. Raatz, I. Dobrinets, M. Lesik, P. Spinicelli, A. Tallaire, J. Achard, V. Jacques, J.-F. Roch, A. M. Zaitsev, J. Meijer, and S. Pezzagna, Phys. Status Solidi A **211**, 2268 (2014).

[43] C. Schreyvogel, V. Polyakov, R. Wunderlich, J. Meijer, and C. E. Nebel, Sci. Rep. **5**, 12160 (2015).

[44] C.-L. Cheng, C.-F. Chen, W.-C. Shaio, D.-S. Tsai, and K.-H. Chen, Diamond Relat. Mater. **14**, 1455 (2005).

[45] S.-Y. Sheu, I.-P. Lee, Y. T. Lee, and H.-C. Chang, Astrophys. J. **581**, L55 (2002).
[46] E. A. Ekimov, P. S. Sherin, V. S. Krivobok, S. G. Lyapin, V. A. Gavva, and M. V. Kondrin, Phys. Rev. B **97**, 045206 (2018).
[47] S. Häussler, G. Thiering, A. Dietrich, N. Waasem, T. Teraji, J. Isoya, T. Iwasaki, M. Hatano, F. Jelezko, A. Gali, and A. Kubanek, New J. Phys. **19**, 063036 (2017).
[48] S. G. Lyapin, A. A. Razgulov, A. P. Novikov, E. A. Ekimov, and M. V. Kondrin, Nanosyst.: Phys. Chem. Math. **9**, 67 (2018).
[49] E. A. Ekimov, S. G. Lyapin, A. A. Razgulov, and M. V. Kondrin, J. Exp. Theor. Phys. **129**, 855 (2019).
[50] P. Giannozzi, S. Baroni, N. Bonini, M. Calandra, R. Car, C. Cavazzoni, D. Ceresoli, G. L. Chiarotti, M. Cococcioni, I. Dabo, A. D. Corso, S. de Gironcoli, S. Fabris, G. Fratesi, R. Gebauer, U. Gerstmann, C. Gougoussis, A. Kokalj, M. Lazzeri, L. Martin-Samos, N. Marzari, F. Mauri, R. Mazzarello, S. Paolini, A. Pasquarello, L. Paulatto, C. Sbraccia, S. Scandolo, G. Sclauzero, A. P. Seitsonen, A. Smogunov, P. Umari, and R. M. Wentzcovitch, J. Phys.: Condens. Matter **21**, 395502 (2009).
[51] E. Londero, G. Thiering, L. Razinkovas, A. Gali, and A. Alkauskas, Phys. Rev. B **98**, 035306 (2018).
[52] A. M. Zaitsev, Phys. Rev. B **61**, 12909 (2000).
[53] M. de Jong, L. Seijo, A. Meijerink, and F. T. Rabouw, Phys. Chem. Chem. Phys. **17**, 16959 (2015).
[54] V. A. Nadolinny, V. S. Shatsky, O. P. Yuryeva, M. I. Rakhmanova, A. Y. Komarovskikh, A. A. Kalinin, and Y. N. Palyanov, Phys. Chem. Miner. **47**, 4 (2020).
[55] A. M. Ferrari, S. Salustro, F. S. Gentile, W. C. Mackrodt, and R. Dovesi, Carbon **134**, 354 (2018).
[56] P. Deák, B. Aradi, M. Kaviani, T. Frauenheim, and A. Gali, Phys. Rev. B **89**, 075203 (2014).
[57] J. P. Goss, P. R. Briddon, and M. J. Shaw, Phys. Rev. B **76**, 075204 (2007).
[58] G. Thiering and A. Gali, Phys. Rev. B **92**, 165203 (2015).
[59] K. Iakoubovskii and A. Stesmans, Phys. Rev. B **66**, 195207 (2002).